Chapter 2

Materials and methods

2.1 Introduction

This chapter provides a detailed account of the steps taken to achieve the objectives. It commences by outlining the design procedure employed for the development of UFG and bulk nanostructured steel. The UFG structure is produced by employing the ECAP method on a low carbon steel. In order to design the bulk nanostructured steel, various thermodynamic-based software tools such as Thermo-Calc and JMatPro are utilized. The alloy is fabricated in-house using an induction furnace, and a final heat treatment is conducted to generate nanostructures. Subsequently, the UFG and nanostructured (NS) steels undergo treatment with high-density current pulses, and a range of characterization techniques are employed to analyse changes in phase, structure, and mechanical properties.

2.2 Effect of alloying elements

To produce bulk nanostructured steel, effects of different alloying elements are considered as given below [146] .

Carbon:

Carbon serves as the primary interstitial solute atom in steel and plays a crucial role in enhancing the material's solid solution strengthening. It effectively lowers the temperature at which martensite and bainite formation begins, leading to the refinement of the microstructural scale. Higher carbon concentrations in austenite enhance its chemical and mechanical stability, preventing its transformation into martensite.

Silicon:

Silicon has the effect of inhibiting the precipitation of cementite, especially during bainite growth from austenite. In the presence of silicon, carbon tends to partition into the austenite phase, stabilizing it at ambient temperature. Silicon effectively supresses the precipitation of

carbides or cementite. A minimum content of silicon of ≈1.5 mass% is required [66]. Silicon has very limited solubility in carbide. The presence of silicon trapped within the carbide significantly reduces the free energy change associated with carbide precipitation. As a result, the precipitation of carbide becomes less thermodynamically favourable.

Manganese:

Manganese plays a crucial role in enhancing the stability of austenite, but it has the effect of shifting the T_o curve to lower carbon concentrations. As a result, the concentration of manganese is typically limited to around 2 mass% to maintain desirable hardenability in steel. Additionally, manganese serves as a strengthening element for ferrite, contributing to the overall strength and mechanical properties of the material.

Cobalt and aluminium:

The bainite transformation at low-temperature is relatively slow. However, the addition of cobalt and aluminium can increase the free energy change associated with the transformation from $\gamma \rightarrow \alpha_b$ transformation and hence can be used to accelerate the rate of reaction. Furthermore, aluminium has the additional benefit of retarding the precipitation of cementite.

Molybdenum:

Molybdenum is added into steel to prevent embrittlement of the austenite grain boundaries caused by impurities like phosphorus. Additionally, molybdenum enhances hardenability and provides a slight improvement in strength. Although molybdenum acts as a ferrite stabilizing element, it can suppress the kinetics of ferrite and pearlite formation. Molybdenum also lowers the bainite start (BS) temperature. The molybdenum content is typically limited to around 0.24 mass% to prevent a significant shift in the T_o curve towards lower carbon concentrations.

Chromium:

Chromium significantly increases the hardenability and decreases the B_S temperature. It also shifts the T_o curve to lower carbon concentrations.

2.3 Materials selection and design

Two different steel compositions are used in this study: one for the development of ultrafine-grained ferrite and the other for the production of nanostructured bainite, martensite, and austenite microstructures.

The steel composition selected for UFG production is designated as D1. The low carbon steel (LCS) is received in the form hot-rolled plate of 330 x 220 x 38 mm^3 dimension from the Research and Development Centre for Iron and Steel, Ranchi, India. The elemental composition of the as-received sample is given in Table 2.1.

The composition of the bulk nanostructured steel is designed using the Java-based material processing (JMatPro) software, which utilizes thermodynamic and kinetics related steel database [147]. The Kirkaldy model is limited to low alloy concentration and based on the work of Zener and Hillert. Later work by Lee and Bhadeshia used different model to give better result for higher concentrations [148]. However, one drawback of these models is the use of dilute solution thermodynamics for calculating transformation temperatures.

When determining the martensite start temperature, the Andrews model is commonly used. However, this model encounters difficulties when the alloy content in the material is high. Ghosh and Olson [149] used T_o concept to solve this problem, but it failed for alloys having M_S temperature below 100 °C. Later, an empirical equation is included in JMatPro for the predictions of M_S temperatures below100 °C.

An alloy (designated as D2) composition, as provided in Table 2.1, is determined based on the considerations and effects of different alloying elements discussed earlier. The stability of various phases in the alloy is calculated using Thermo-Calc software, and the results (Figure 2.1a) indicate that single-phase austenite remains stable above 930 °C. A Time-Temperature-Transformation (TTT) diagram is plotted using the JMatPro software, as shown in Figure 2.1b. Based on the calculations, the approximate start temperatures for bainite and martensite are found to be 333 °C and -8.2 °C, respectively.

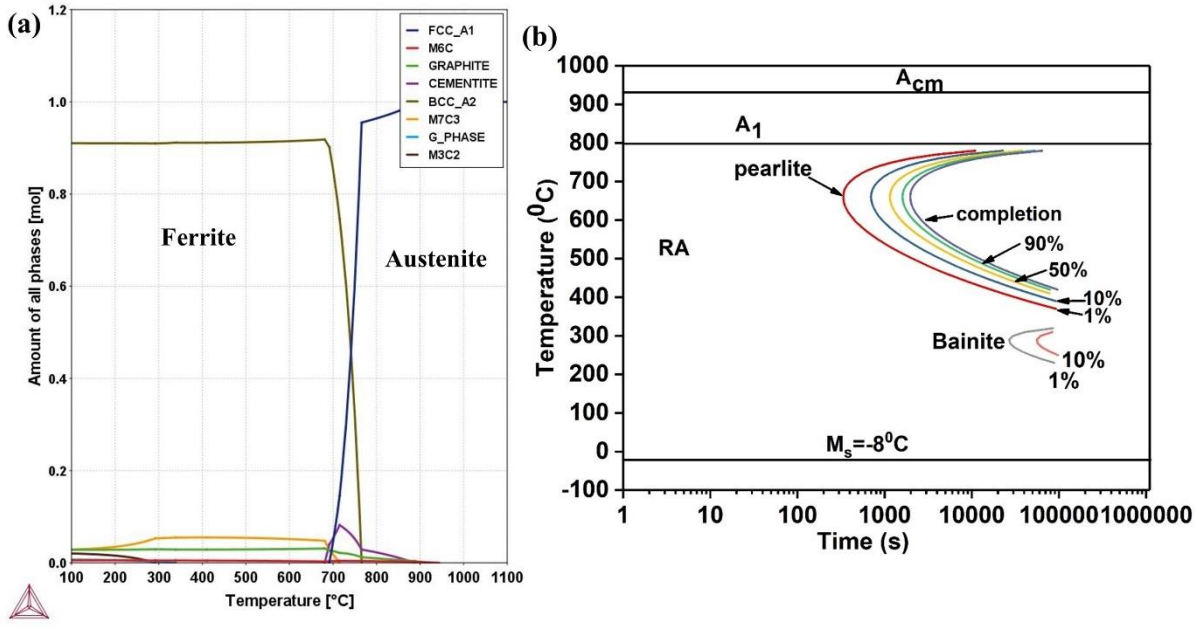

Figure 2.1. (a) *Phase stability diagram calculated using Thermo-Calc and* ***(b)*** *TTT diagram of the D2 steel plotted using JMatPro software, austenitizing temperature of 970°and grain size of ASTM 6.*

Table 2.1. Chemical composition of the two selected materials (mass %).

Element	Fe	C	Si	Mn	Cr	Mo	Co	Al	Ni
D1	Bal.	0.08	0.09	0.3	-	-	-	0.03	-
D2	Bal.	1.06	2.1	2.08	1.3	0.28	1.5	1.2	0.44

2.4 ECAP of D1 sample

Cylindrical workpieces of 15 mm diameter and 80 mm length are machined from the hot-rolled plate in the rolling direction. The workpieces are severely deformed by ECAP technique using a die made up of H11 steel, of hardness ~ HRC 55. The die used for this process has an inner intersection angle of 120° and outer arc angle of 60° as shown in Figure 2.2. The B_C route is adopted to process the samples, in which the sample is rotated 90° about its axis in the same direction between two consecutive passes. The ECAP is carried out at room temperature using a hydraulic press of 30-ton capacity and a ram speed of 60 mm/ min. The ECAP introduces an equivalent strain of 0.6 in the sample by every passage of work pieces through the die. The samples are ECAPed for ten passes, which builds in an equivalent von Misses strain of 6. Strips of dimension 65 mm x 8 mm x 2 mm are machined from the ECAPed samples and designated as ECAP-6. In addition, a set of ECAP-6 samples are subjected to isothermal heat treatment at 200 °C for 5 minutes and 1-hour durations, followed by air cooling. Theses samples are designated as ECAP-6-H1 and ECAP-6-H2 respectively, based on the annealing times.

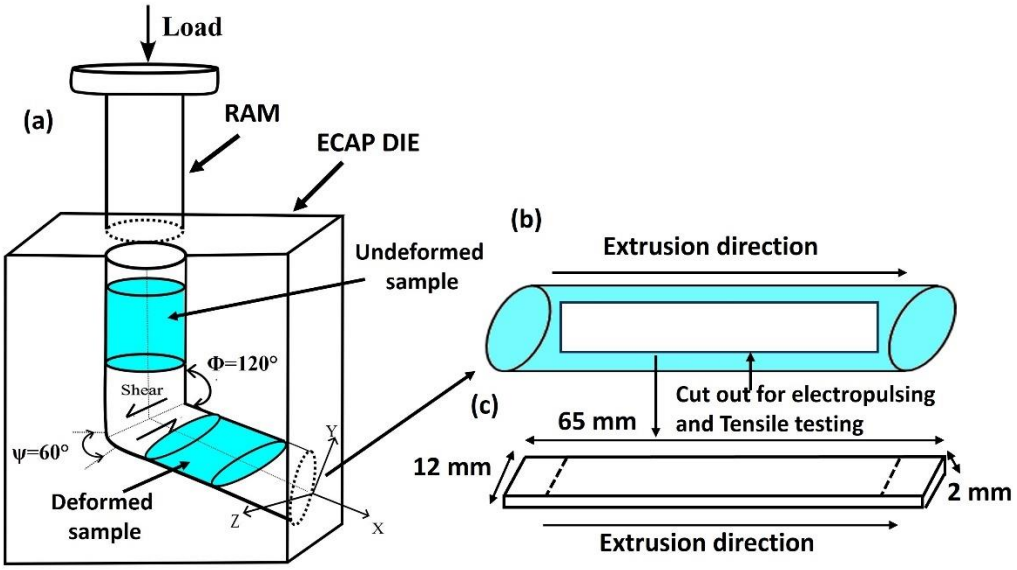

Figure 2.2. *Schematic of* ***(a)*** *ECAP die with work pieces,* ***(b)*** *ECAPed work piece and* ***(c)*** *the cut-out plate from the ECAPed sample.*

2.5 Making of alloy D2

A 2.5 kg alloy is melted using an induction furnace (INDUCTOTHERM, 15 kW, 10 kHz) in the presence of air. The raw materials are melted in a magnesia crucible with a diameter of 65 mm and a length of 150 mm at a temperature of 1575 °C. The iron containing high carbon and other high melting point elements like Nickel or ferro alloys of ferrochrome and ferromolybdenum are melted first followed by ferrosilicon and Aluminium. Finally, manganese is added in its molten form, and after allowing sufficient time for proper mixing, the alloy is cast in a copper mould (Figure 2.3a). The resulting cast plate has dimensions of 150 mm x 100 mm x 15 mm (Figure 2.3b). Bars with dimensions of 100 mm × 10 mm × 10 mm are cut from the cast plate for hot-rolling. The hot-rolling process involves heating the bars for 1 hour at 1000 °C to achieve a 75% reduction in thickness, followed by air cooling. The final composition, as given in Table 2.1, is determined using optical emission spectroscopy of the hot-rolled strips. After hot-rolling, the material is further machined to dimensions of 65 mm x 12 mm x 2 mm for additional processing.

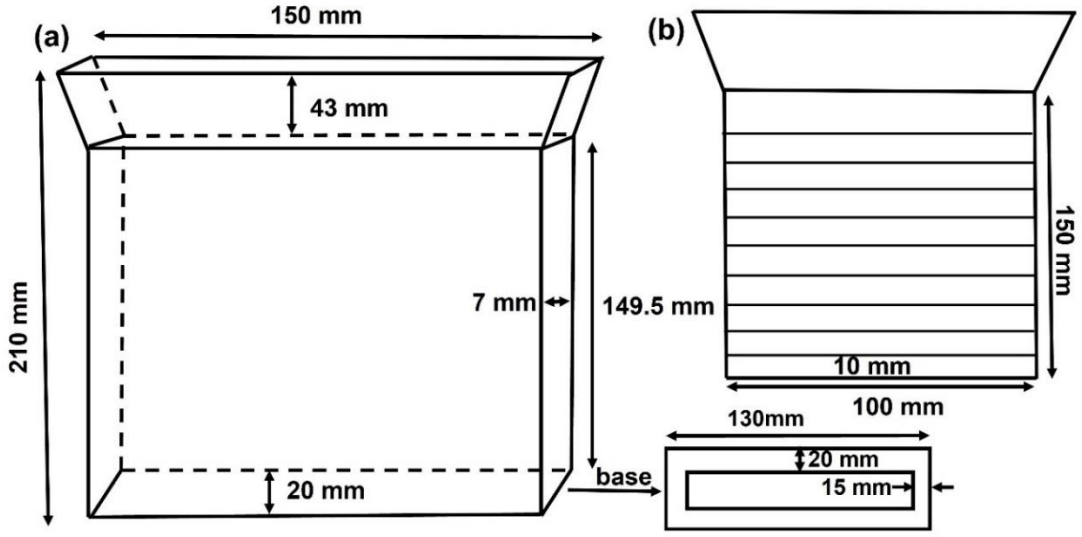

Figure 2.3. (a) *Schematic diagram of casting and* ***(b)*** *elevation of cast plate.*

2.6 Heat treatment

Based on the TTT diagram plotted using JMatPro software (Figure 2.1b), a temperature of 250 °C is selected for the austempering process to achieve nanostructured bainite. The bainitic transformation timings for 1 percent and 10 percent are calculated using the TTT curve. Based on this data, two approximate timings of 25 hours and 48 hours are chosen to produce two different volume fractions of bainite, both with significant amounts of retained austenite (RA). Samples with dimensions of 65×12×2 mm^3 are austenitized at 970 °C for 30 minutes in a vacuum-sealed quartz tube. The austenitized samples are removed from the tube and austempered at 250°C in a salt bath of 50% KNO_3 and 50% $NaNO_2$ for 25 hours and 48 hours, followed by air cooling. The heat treatment cycles are shown in Figure 2.4. The austempered samples for timings 25 hours and 48 hours are designated as D2-25h and D2-48h, respectively.

Another batch of hot-rolled samples is prepared by vacuum-sealing them in quartz tubes. These samples are then austenitized at 970 °C for 30 minutes and subsequently allowed to cool to ambient temperature after breaking the tube seal. The heat treatment cycle for this process is depicted in Figure 2.4, and the samples are designated as D2-A.

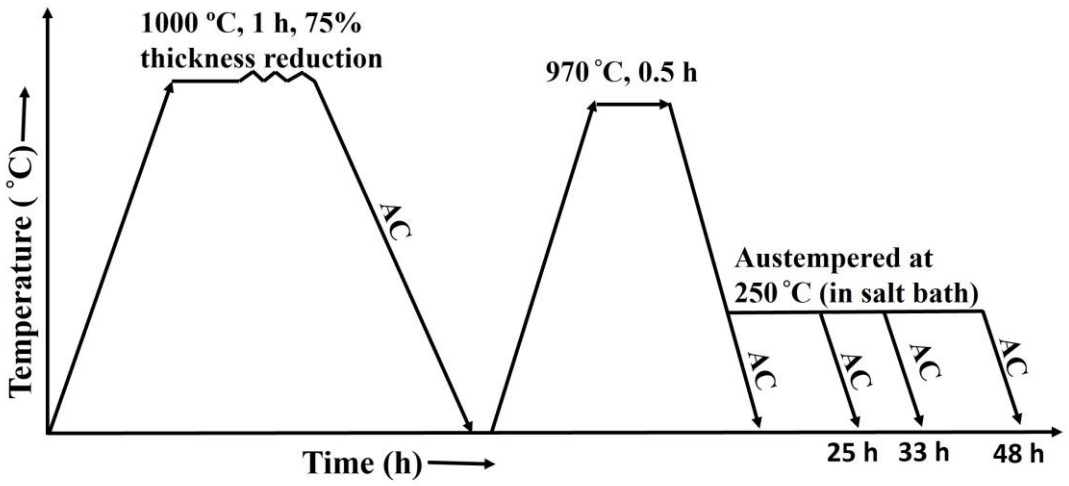

Figure 2.4. *Thermal cycles for hot-rolling, austenitization followed by air-cooling and austempering at 250°C.*

2.7 Electropulsing

A schematic diagram of electropulsing operation is shown in figure 2.5a. An input power of 415V AC, 50Hz is supplied to capacitor-charging power supply (CCPS) at 20A rate to attain the set voltage. The CCPS charges capacitor bank at the rate of 200 mA DC with a step up voltage and the bank can store a maximum power of 39 kJ energy at a rate of 2.8 kJ/s through a protection circuit. The capacitor bank is made up of 14 numbers of parallel-connected capacitors, each with a capacity of 14 µF and a 20 kV voltage and the assembly has a total capacitance of 196 µF. A single trigatron type spark gap is attached to the output of capacitor bank and sample load to use as switch. A trigger generator provides trigger pulse for firing the spark gap when master trigger command is activated. It closes the spark gap switch that sends high power to the load cell/ sample. Current is measured through a Rogowski coil with the help of cathode ray oscilloscope. The output current displays as a damped oscillation as shown in figure 2.5b.

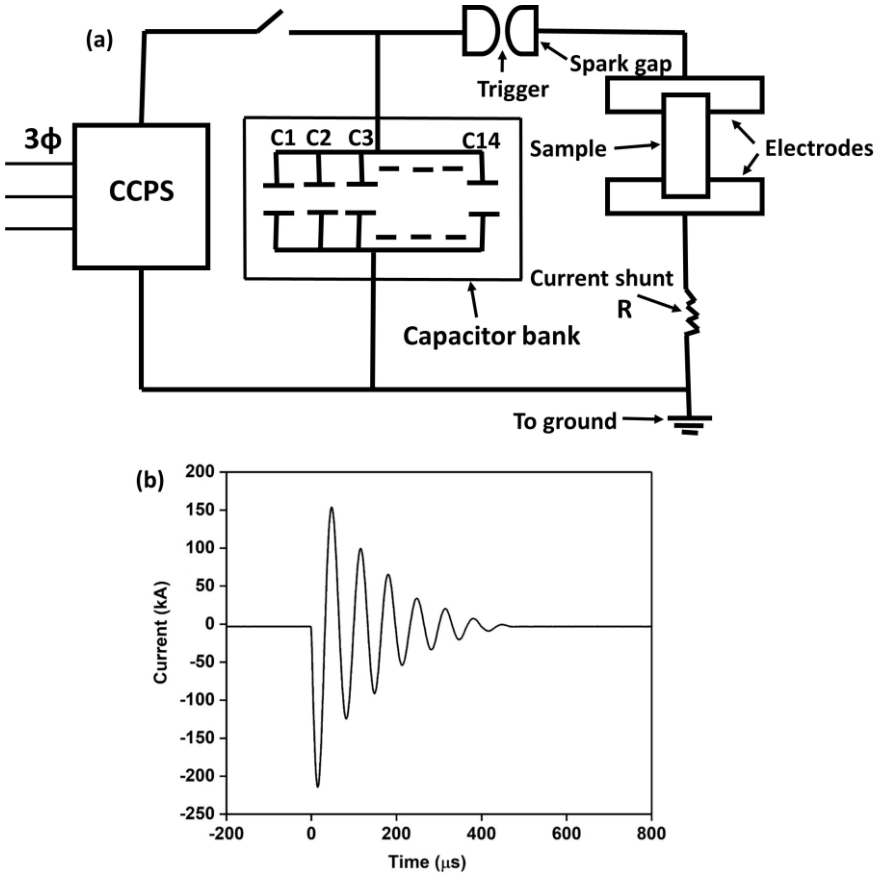

Figure 2.5. (a) *Schematic diagram of electropulsing set up and* ***(b)*** *Waveform of the electric pulse.*

The circuit diagram of experimental set up for EP and sample holding position are shown in Fig. 2.5a and b respectively. The plate shaped specimen (Fig. 2.5c) of air cooled (D2-A), austempered (D2-48h) and equal-channel angular pressed (ECAP-6) samples are further subjected to EP for different current densities and times as given in Table 2.2. The equal- channel angular pressed samples electropulsed for one time and repeatedly for five times are designated as ECAP-6-EP-1 and ECAP-6-EP-5, respectively. The D2-48h samples are electropulsed at a higher current density for one pulse and also repeatedly for five pulses, designated as D2-48h-EP-1 and D2-48h-EP-5, respectively. Another D2-48h sample is electropulsed for one time at a lower current density and designated as D2-48h-EP-1-LCD. Similarly, the D2-A sample is electropulsed at higher and lower current densities and designated as D2-A-EP-1 and D2-A-EP-1-LCD, respectively.

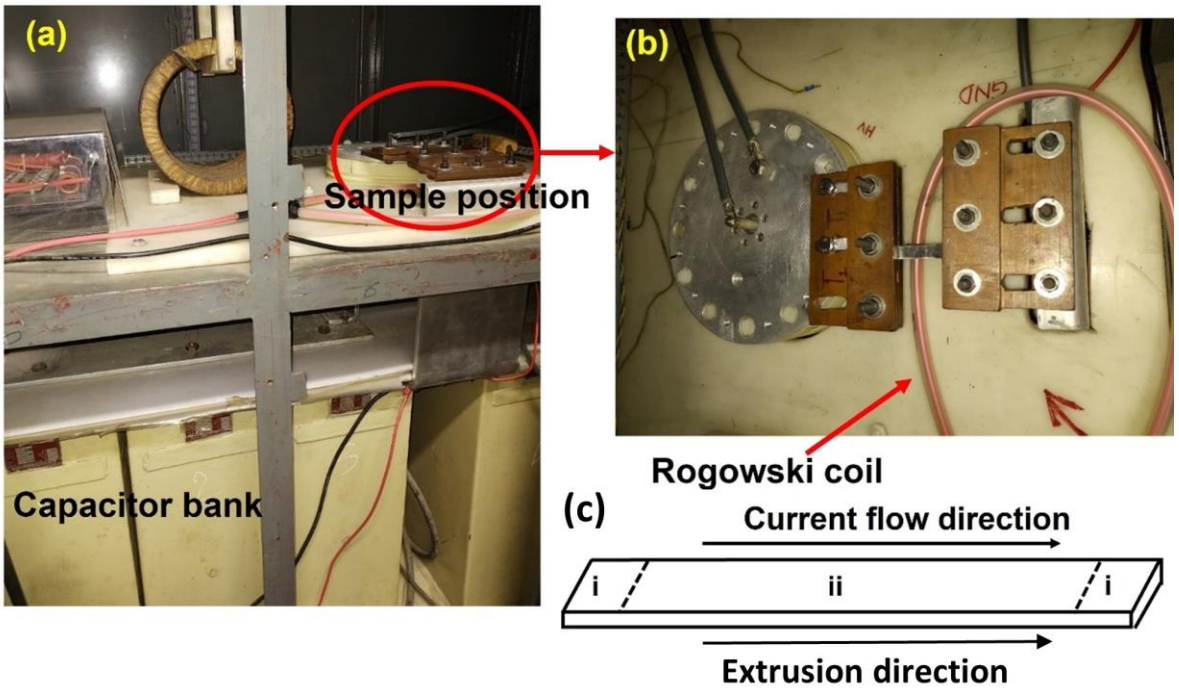

Figure 2.6. (a) *Electropulsing set up,* ***(b)*** *sample holding position between electrodes and* ***(c)*** *schematic diagram of sample for electropulsing (arrow showing current flow direction),* ***(i)*** *clamping region* ***(ii)*** *area for microstructural characterization.*

Table 2.2. Details of EP parameters

Sample designation	Voltage (kV)	No of pulses	Time period (μs)	Frequency (kHz)	Total Discharge time (μs)	Peak Current density (kA/mm^2)
ECAP-6-EP-1	10	1	52	19.2	358	14.25
ECAP-6-EP-5	10	5	52	19.2	358	14.25
D2-48h-EP-1	14	1	65.7	15.2	511	8.8
D2-48h-EP-5	14	5	65.7	15.2	511	8.8
D2-48h-EP-1-LCD	5	1	52	19.2	358	6.3
D2-A-EP-1	14	1	65.7	15.2	511	8.8
D2-A-EP-1-LCD	5	1	52	19.2	358	4.8

2.8 Microstructural characterization

2.8.1 Optical and scanning electron microscopy

Optical microscopy is conducted to examine the morphology of different phases. The samples undergo grinding and polishing with 0.3 μm alumina powder to achieve a mirror finish. Subsequently, they are etched in a 2 percent nital solution before examination using a Zeiss Metalux-3 optical microscope.

Additionally, the lightly etched samples are investigated through secondary electron imaging using an FEI Quanta 200FEG scanning electron microscope (SEM). The SEM is employed to observe the morphology of bainite and austenite and to measure the thickness of bainite plates.

2.8.2 X-ray diffraction

The samples are scanned using Co-Kα (λ=1.789 Å) radiation in a Malvern Panalytical Empyrean model X-ray diffractometer. The X-ray diffraction (XRD) measurements are performed within an angular range of 40° to 130°, with a scanning speed of 2°/min and a step size of 0.01°. Phases are identified using the ICDD PDF2 database. For quantitative phase fraction and lattice parameter determination, the Rietveld refinement technique is employed on

the XRD patterns using High score plus software version 5 [150–152]. In this technique, an intensity profile is calculated and fitted with the observed experimental spectrum through a least-square iterative process [151]. The refinement process incorporates crystal structure data, such as lattice parameters, space group, site occupancy, temperature factor, and scan parameters like wavelength, Lorentz-Polarization factor, slit width, etc. The quality of the fit is assessed by minimizing the function Δ, which is the summation of the weighted fraction of least-squared errors. This can be expressed as given in Equation 2.1

$$\Delta = \sum_i w_i[y_i(obs) - y_i(calc)]^2 \qquad (2.1)$$

where, i is the number of steps, y_i (obs) and y_i ($calc$) are the observed and calculated intensities respectively at each i^{th} step, w_i is a weight factor which is inverse of y_i (obs) applied to each i^{th} scattering angle. Various methods assess the quality of the fit of the calculated pattern to the observed data. Here, the key parameters R-weighted pattern (R_{wp}) value and R-expected (R_{exp}) values are calculated from Equation 2.2 and Equation 2.3 respectively [153].

$$R_{wp} = \{\sum_i w_i[y_i(obs) - y_i(calc)]^2 / \sum_i w_i[y_i(obs)]^2\}^{1/2} \qquad (2.2)$$

$$R_{exp} = [\frac{(N-P)}{\sum_i^N W_i Y_i(obs)^2}]^{1/2} \qquad (2.3)$$

where N is the number of observations and P is the number of parameters. The goodness of fit (χ) is given by Equation 2.4.

$$\chi^2 = \frac{\Sigma W_i(y_{io} - y_{ic})^2}{N-P} = [\frac{R_{wp}}{R_{exp}}]^2 \qquad (2.4)$$

The goodness of fit (GOF), χ^2 should be within the range 1 and 4 for best fit.

Crystallite size (B) and microstrain (ε_m) are calculated using Scherrer formula as given in Equations (2.5) and (2.6), respectively [154].

$$B = \frac{S\lambda}{\Delta K_c cos\theta} \qquad (2.5)$$

$$\Delta K_c = 4\varepsilon_m tan\theta \qquad (2.6)$$

The symbol *S* is Scherrer constant, ΔK_c is the broadening of a XRD peak after subtracting from instrumental broadening. The broadening is determined after fitting the XRD peaks with Pseudo-Voigt function [155]. Broadening due to the instrument is determined using standard Si sample and subtracted from the experimental value.

The lattice parameter values obtained from Rietveld refinement are used to calculate carbon content in retained austenite (RA) using Equation 2.7 [156,157].

$$a_\gamma(nm) = 0.356 + 0.00453w_C + 0.000095w_{Mn} + 0.00056w_{Al} + 0.0006w_{Cr} - 0.0002w_{Ni} \qquad (2.7)$$

where a_γ is lattice parameter of austenite in nm and $w_C, w_{Mn}, w_{Al}, w_{Cr}, w_{Ni}$ are mass % of carbon, manganese, aluminum, chromium, and nickel, respectively. The lattice parameter of bainite is calculated from the empirical Equation 2.8 [158] .

$$a_\alpha = 2.8664 + 0.039w_C + 0.0006w_{Mn} + 0.00185w_{Si} \qquad (2.8)$$

where a_α is lattice parameter of bainite in Å and w_{Si} is mass % of Si.

Usually, the Williamson-Hall (WH) method is used to compute the dislocation density (ρ) with the assumption that the material is isotropic. The dislocation density is mainly related with peak width and other factors as given in Equation 2.9 [159,160].

$$\Delta K \simeq \frac{S}{B} + Zb\sqrt{\rho}K_d \qquad (2.9)$$

where ΔK is the peak width ($\Delta K = \frac{2cos\theta(\Delta\theta)}{\lambda}$), Z is a constant (0.263), K_d is the diffraction vector ($K_d = \frac{2sin\theta}{\lambda}$), b is the Burgers vector and ρ is the dislocation density. From the slope of the straight-line plot between ΔK and K_d at different planes, dislocation density can be calculated. But this is an ideal case where no strain anisotropy is present in the material.

However, in reality the material always exhibits strain anisotropy. Therefore, the modified Williamson-Hall method (MWH) [161,162], is adopted to calculate dislocation density considering the dislocation contrast factor to take care of the anisotropy. The full width at half maximum intensity of the diffraction peak in the MWH method is correlated to dislocation density (ρ) as given by Equation 2.10.

$$\Delta K \simeq \frac{S}{t} + Mb\sqrt{\frac{\pi}{2}\rho}\, K_d \bar{C}^{1/2} \qquad (2.10)$$

where *M* is the dislocation screening parameter, $\bar{C}$ is dislocation contrast factor which is related to other parameters as given in Equation 2.11 [162].

$$\bar{C} = \bar{C}_{h00}(1 - qH^2) \qquad (2.11)$$

The parameters $\bar{C}_{h00}$ and H^2 are determined using the method described in reference [162]. Combining Equations 2.10 and 2.11, the modified equation can be rewritten as given Equation 2.12 given below.

$$\frac{(\Delta K - \alpha)^2}{K_d^2} \cong \beta^2 \bar{C}_{hoo}(1 - qH^2) \qquad (2.12)$$

Here α is given as $\frac{S}{t}$, β is $Mb\sqrt{\frac{\pi\rho}{2}}$. The value of q in the above equation is determined by plotting H^2 versus left side of the equation and finding the point where the line intersects the horizontal axis. *M* is taken as 0.4 for austenite and 1.4 for bainite [159,163]. Instead of ΔK vs K_d, linear fitting is carried out between ΔK vs $K_d \bar{C}^{1/2}$ and dislocation density is calculated from the slope, $Mb\sqrt{\frac{\pi}{2}\rho}$.

2.8.3 Transmission electron microscopy

The samples are initially sliced using a diamond wafering blade into a thickness of 0.5 mm. Subsequently, these slices are ground down by alumina-based abrasive papers to obtain a

thin foil with a thickness of 50 µm. From this foil, discs with a diameter of 3 mm are punched out and then subjected to electropolishing in a Tenupol-5 Struers twin jet electropolisher. The electropolishing process utilizes an electrolyte of 5% perchloric acid in methanol at a temperature of -30°C (243K) and a voltage of 40 kV.

Electropolished discs are investigated in a transmission electron microscope (TEM) using a Tecnai $20G^2$ and JEOL 2200 FS model operating at a voltage of 200 keV for detailed microstructural and phase analysis.

2.8.4 Electron back scattered diffraction

Rectangular strips with dimensions of 12 mm x 10 mm x 2.5 mm are mechanically ground and polished using alumina powder. The samples are further polished in vibromet using colloidal silica with a size of 0.3 µm. The polished samples are scanned for electron back-scattered diffraction (EBSD) study using a Quanta 3D FEG SEM at an accelerating voltage of 20 kV, a working distance of 15 mm, and a tilting angle of 70°. The step size of the scanning is taken 50 nm. The scanned data are cleaned with a grain tolerance angle lower than 2° and a confidence index lower than 0.1. The cleaned data are then analysed for inverse pole figure (IPF), image quality (IQ) map, Kernel average misorientation (KAM), misorientation angle (MA) distribution, grain size distribution, phase map and orientation relationship between parent and product phases using TSL OIM version 8 software.

2.9 Mechanical properties

Flat tensile specimens of gauge length 10 mm and gauge width 4 mm are prepared according to ASTM-E8 standards. Tensile testing for both the specimens is conducted at room temperature using an Instron 8862 model of 100 kN capacity at a crosshead speed of 1 mm per minute.

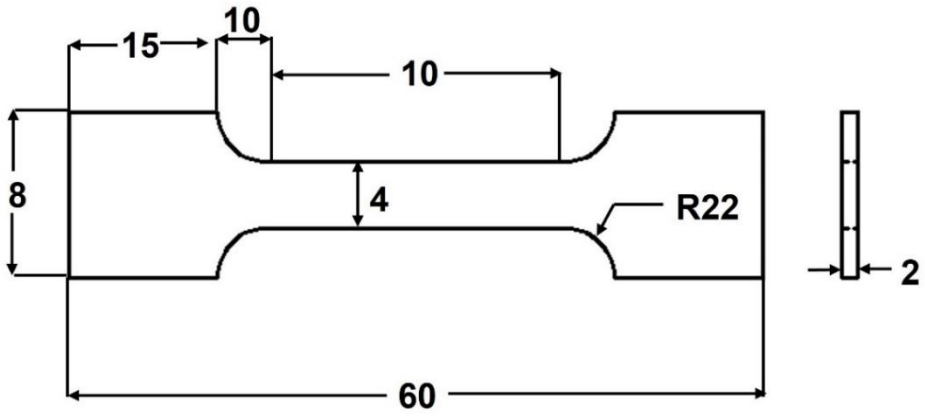

Figure 2.7. *Schematic drawing of the tensile sample (all dimensions are in mm).*

The yield strength, ultimate tensile strength, uniform elongation (UE), and total elongation (TE) are estimated from the load-elongation data. True stress-true strain data are calculated from the engineering stress-engineering strain data. The logarithm true stress vs logarithm true plastic strain graph is also plotted and fitted using various work hardening models like Hollomon [164], which describes work hardening for single slope as given in Equation 2.13.

$$\sigma = K\varepsilon^n \qquad (2.13)$$

where σ is true stress, ε is true strain, K is the strength coefficient and n are the work-hardening exponent

The basic equation for metals with variable yield strength and work hardening behaviour can be better fitted by Ludwik [165] equation as given in Equation 2.14.

$$\sigma = \sigma_o + K\varepsilon^n \qquad (2.14)$$

Materials with pre-strain are generally fitted with the Swift model [166] (Equation 2.15), whereas for the saturation stress Voce model [167] is used (Equation 2.16).

$$\sigma = K(\varepsilon_o + \varepsilon)^n \qquad (2.15)$$

$$\sigma = \sigma_s - (\sigma_s - \sigma_{it})(n\varepsilon) \qquad (2.16)$$

The work-hardening behaviour of face centred cubic metals with low stacking fault energy is explained using the Ludwigson equation [168] (Equation 2.17).

$$\sigma = K\varepsilon^{n} + \exp(K_1 + n_1\varepsilon) \qquad (2.17)$$

where σ_o is the stress at yielding, ε_0 is pre-strain, σ_s is the saturation stress and σ_{it} is the true yield stress, K_1 represents the additional strength coefficient, and n_1 is the additional work-hardening exponent.

The Levenberg Marquardt iteration algorithm is used to find the best fit. The best fit is determined by the lowest value of $\chi 2$ or the highest value of adj. R^2. The work hardening parameters are derived by the above iteration technique from the best-fit curve/equation. Work hardening rate vs true plastic strain is also plotted to find the possible deformation mechanisms.

Microhardness is measured using instrumented model MHT3 of Anton Paar applying a force of 5000 mN and a dwell time of the 20 seconds. Applied force vs depth of indentation is also plotted.